AIAA JOURNAL
Vol. 50, No. 12, December 2012

Shockwave/Boundary-Layer Interaction Control on a Compression Ramp Using Steady Microjets

S. B. Verma* and C. Manisankar†
National Aerospace Laboratories, Bangalore 560 017, India

DOI: 10.2514/1.J051577

An experimental investigation was conducted to control the amplitude of shock unsteadiness associated with a 24 deg compression-ramp-induced interaction in a Mach 2 flow. Two control configurations in the form of an array of 1) 16 90-deg-pitched steady micro-air-jet vortex-generating devices (AJVG1), and 2) eight pairs of 45-deg-pitched steady micro-air-jet vortex-generating devices (AJVG2) were studied. Each AJVG device was placed upstream of the interaction region at 12.5δ from the compression corner. Both micro-AJVG configurations show a reduction in separation shock strength and help considerably reduce the height of the lambda-wave triple point with increase in P_{oj}. Pitching the microjets at 45 deg, as in the AJVG2 configuration, prevents a stronger control-generated bow shock to form ahead of the injectors and, hence, reduces the obstruction component of the interaction significantly. A well-defined separation line for no control is seen to get replaced by a highly corrugated separation line with control. Significant reduction (up to 67%) in the peak rms value is observed in the intermittent region of separation with AJVG1 for $P_{oj} \geq 208.5$ kPa while the same is achieved with AJVG2 at a much higher P_{oj} (>500 kPa). The spectral content of the pressure fluctuations also indicate that, relative to the AJVG2 configuration, AJVG1 is successful in reducing the amplitude of fluctuations in the range of unsteadiness by an order of magnitude as soon as P_{oj} exceeds 208.5 kPa. The amplitude of these fluctuations is seen to further decrease with increase in P_{oj}.

Nomenclature

d	=	diameter of the air jet, mm
f_s	=	characteristic frequency of structures in incoming boundary layer, Hz
$G(f)$	=	power spectral density, kPa^2/Hz
L	=	length of the flat plate, mm
l	=	distance between the air jets of a single unit, mm
M_j	=	sonic jet exit Mach number
M_∞	=	freestream Mach number
P_j	=	air-jet exit pressure, kPa
P_{oj}	=	air-jet stagnation pressure, kPa
P_w	=	mean wall pressure, kPa
P_0	=	tunnel stagnation pressure, kPa
P_∞	=	freestream static pressure, kPa
q	=	$(P\gamma M^2)_j/(P\gamma M^2)_\infty$, momentum flux ratio
U_e	=	external cross-flow velocity, m $\cdot$ s^{-1}
U_j	=	calculated equivalent jet exit velocity, m $\cdot$ s^{-1}
X	=	coordinate in the streamwise direction
X_d	=	depth of the corrugation
Y	=	coordinate in the transverse direction
Y_1	=	height of the Mach disk, mm
Z	=	coordinate in the vertical direction
α	=	skew angle of the air jets, deg
β	=	pitch angle of the air jets, deg
δ	=	boundary-layer thickness, mm
ζ	=	control-generated wave turning angle, deg
λ	=	distance between two air jet units, mm
θ	=	compression ramp angle, deg
σ/P_w	=	nondimensionalized local rms value
$\sigma_{\max}/P_w$	=	nondimensionalized peak rms value in the intermittent region of separation

Received 25 August 2011; revision received 19 January 2012; accepted for publication 7 February 2012.

*Principal Scientist, Council of Scientific and Industrial Research, Experimental Aerodynamics Division; sbverma@ead.cmmacs.ernet.in. Senior Member AIAA.

†Scientist, Council of Scientific and Industrial Research, Experimental Aerodynamics Division; mani@nal.res.in.

I. Introduction

SHOCK-WAVE/BOUNDARY-LAYER interaction (SWBLI) in supersonic flow is initiated by the strong adverse pressure gradient imposed by the interacting shock on the incoming boundary layer that leads to flow separation (Fig. 1). The process of separation is generally associated with low-frequency oscillations of the separation shock (with frequencies lower than the temporal scales of the incoming flow [1,2]) and results in an increase in flow unsteadiness in the region of influence (which, in turn, is found to increase with increase in shock strength or intensity [3–5]). As such, the region of flow interaction is subject to increased aerodynamic drag, heat transfer, and unsteady pressure loads, and hence these are important design factors [3]. Much of the early work on SWBLI [2–9] was focused on understanding the dynamic/unsteady behavior of these interactions and identifying its causes. Various mechanisms, identifying the source of the low-frequency pulsations, have been proposed in literature. These primarily include those that are caused either by the upstream conditions in the incoming boundary layer [10,11] or by the downstream conditions in the separated region [12]. According to the latter model, the flow in these interactions becomes unsteady when the pressure ratio across the oblique shock is such that the mass of the fluid reversed at the reattachment point does not balance the scavenged fluid from the separation region [12,13]. As a result, the separated region 'breathes' and, during one-half of the pulse, mass is injected into it, while during the other half it is ejected out, resulting in an unsteady mass exchange [12]. This sets the shock system into low-frequency oscillations, causing detrimental unsteady fluctuations that exhibit a wide range of spatial and temporal scales [4]. Flow-control techniques have therefore been suggested [4] as an important design issue to mitigate or negate these adverse effects.

Recently, exploratory studies have been carried out to diminish the detrimental effects of SWBLI using flow control by altering the characteristics of the incoming boundary layer, such as introducing fullness to the velocity profile [14]. In general, flow-control techniques rely on the generation of vortices near the wall by the use of either static systems or mechanical vortex-generating (VG) devices such as microramps, vane-type VG fixed at an angle to the

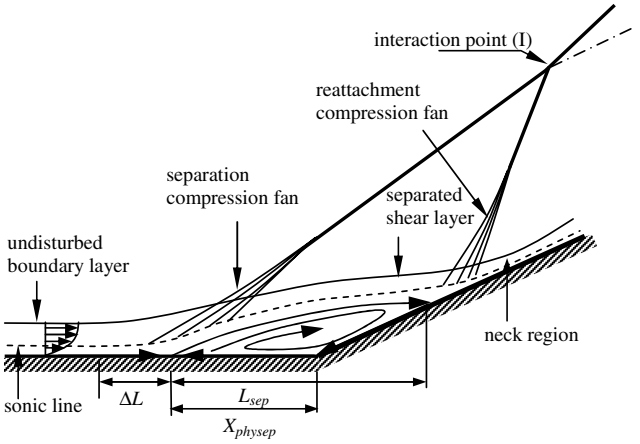

Fig. 1 Schematic showing the important flow features of the shockwave/boundary-layer interaction phenomena over a compression corner.

main flow [14–17], steady micro air jets [18–26], or pulsed-jets using actuators [27,28], at an appropriate distance upstream of the region of interaction. The aim in either case is to reduce the shock strength and, hence, reduce wave drag or reduce the extent of separation with the aim of reducing shock unsteadiness or both [29]. Such studies are relevant to air inlets so as to increase mass-flow ingestion, resulting in enhanced inlet operability and, therefore, improve overall engine performance. Although mechanical VG devices are a better choice due to their ruggedness and, hence, less chance of mechanical failure [14,30], air-jet control methods have the added advantage of integrating flow control with transpiration cooling [22] and the additional feature of switching it on and off [14]. These devices generate either corotating or counter-rotating vortices, depending upon their design and angular positions with respect to the main flow direction. The optimization procedure in this case involves studying jet inclination effects and the associated strength of vortex generated [18,24]. The spanwise spacing between the VG devices has also been an important parameter in controlling the flow interaction. Recent studies [15,16,19] have also revealed that sub-boundary-layer control devices (i.e., with h/δ of 0.1–0.4) to be more effective in suppressing control-generated wave drag and stabilizing the interaction region relative to conventional VG devices. Further, the choice of placement location of the VG devices depends primarily on the type of interaction and the flow Mach number. In contrast to mechanical vortex generators, an air-jet control device enables enhanced penetration of the vortices through the severe adverse pressure gradients that introduce excess momentum along the core of the vortices [19,20].

Although a lot of studies have demonstrated the effectiveness of air jets in positively controlling the flow, most of these have been in the incompressible/subsonic regimes, with relatively few in transonic/supersonic interactions. The present paper reports the results of an exploratory study conducted to control the amplitude of shock unsteadiness associated with the SWBLI on a 24 deg compression corner using an array of 1) 90-deg-pitched steady micro air jets, and 2) pairs of 45-deg-pitched (arranged in counter-rotating configuration [26]) steady micro-air-jet vortex-generating (AJVG) devices. The former arrangement has an array of 16 micro air jets (spaced $10d$; $d = 0.6$ mm) while the latter has eight pairs of counter-rotating micro-AJVG devices, each spanning the width of the plate and introduced upstream of the interaction. The primary objective was to study the effect of 1) pitch angle β of micro air jets and 2) air-jet supply pressure P_{oj} on the amplitude of pressure fluctuations in the intermittent region of separation for compression ramp angles θ of 20, 22, and 24 deg, respectively. Detailed investigation of the interaction is made using color schlieren, real-time pressure measurements using fast piezoresistive Kulite pressure sensors and surface-oil visualization.

II. Experimental Setup and Procedure

A. Wind Tunnel Facility and Model Details

Tests were conducted in the 0.46×0.3 m blowdown tri-sonic wind tunnel at National Aerospace Laboratories. The compression corner model was mounted on a sting along the tunnel centerline to avoid effects of noise levels from the turbulent boundary layer generally present on wind-tunnel walls. The freestream Mach number M_∞ was 2.05 ± 0.02, while the stagnation pressure P_0 and temperature T_0 were 208.5 kPa $\pm$ 2% (absolute) and 298 K$\pm$ 0.4%, respectively. This gives a unit Reynolds number of 25.257×10^6 m^{-1}. The wall temperature was approximately adiabatic. The flat plate of the model is 28 cm long with a span of 11 cm (Fig. 2) and has a provision to change the ramp angle θ (in steps of 2 deg) between 16 and 24 deg. The Reynolds number based on the plate length distance is 7.07×10^6. No side fences are used to facilitate schlieren imaging. A boundary-layer trip, made of 60 grit carborundum particles spanning 4 mm in length and placed at 17 mm from the leading edge (Fig. 2) is used to ensure a sufficiently thick turbulent boundary layer.

Control devices in the form of an array of steady sonic micro air jets are used to modify the flow interaction. Figures 3a and 3b show the schematic of the two micro-AJVG configurations used in the present study. These configurations were primarily chosen to study the effect of pitch angle β of air jets in controlling the amplitude of shock unsteadiness in the intermittent region of separation. Here, the pitch angle β is defined [21] as the angle between the jet-hole centerline and the wall, as shown in Fig. 4. In the first arrangement (AJVG1), the array consists of 16 steady sonic micro air jets pitched at 90 deg ($d = 0.6$ mm and with an inter-jet spacing of $10d$), Fig. 3a, while the second arrangement (AJVG2) consists of eight pairs of 45-deg-pitched steady sonic micro air jets in counter-rotating configuration [26] (Fig. 3b). In the latter arrangement, because the jet is pitched at 45 deg with respect to the wall, the opening at the wall surface (i.e., the jet hole) is an ellipse. The skew angle α, in this case, can be thought of as the angle between the major axis of the ellipse and the streamwise direction (Fig. 4) [21]. In both the micro-AJVG configurations tested, the skew angle α of the jets is kept as 90 deg. These micro-AJVG devices are introduced upstream of the interaction (50 mm upstream of the compression corner), as shown in

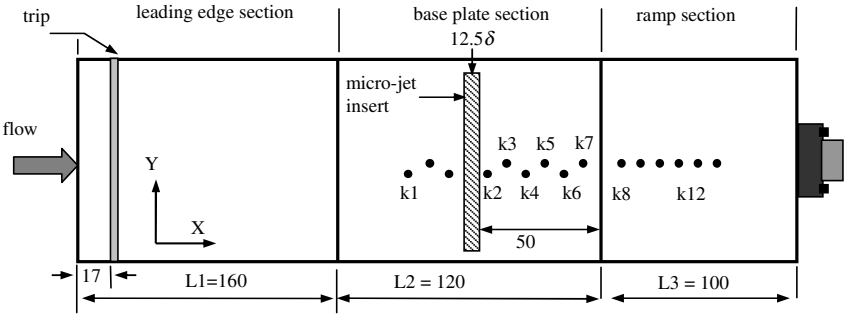

Fig. 2 Schematic showing the compression ramp model details with the pressure sensor locations; AJVG location 12.5δ. All dimensions are in millimeters.

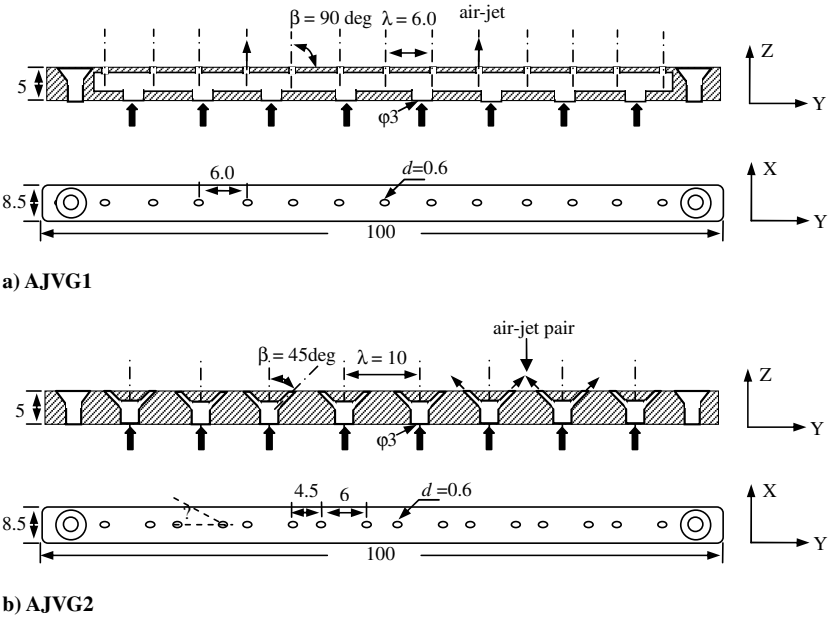

Fig. 3 Schematic of the air-jet vortex-generating configurations: a) 90-deg-pitched steady air-jet configuration (AJVG1), and b) 45-deg-pitched steady air-jet configuration (AJVG2) arranged in counter-rotating configuration [26]. All dimensions are in millimeters.

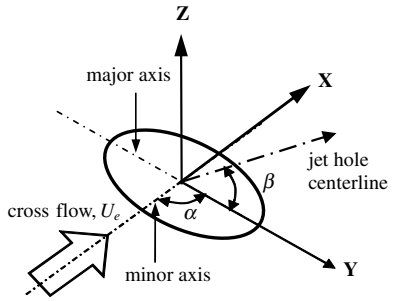

Fig. 4 Choice of axis and the coordinate system showing the pitch (β) and skew (α) angles for the AJVG2 configuration.

Fig. 3a, where the boundary-layer thickness is approximately 3.85 mm. With respect to the interaction location (approximately 20 mm upstream of corner where $\delta = 4.0$ mm), this location corresponds to 12.5δ. The boundary-layer thicknesses were estimated based on length Reynolds number Re_x for turbulent flows and then corrected for compressible flows as per the procedure suggested by Van Driest [31] and Verma and Gupta [32] for Mach number greater than unity. It may be noted, however, that such an estimation may differ from the boundary-layer thickness calculated from velocity profile by $\pm 3\%$ [33]. Assuming [34] transition to occur at about 1.1×10^6, the length Reynolds number (of 4.04×10^6) suggests the boundary layer to be fully developed about 50 mm or 13δ upstream of the microjet insert. The freestream velocity U_e of the cross flow was 523 $\mathrm{m \cdot s^{-1}}$. The Reynolds number of the jet, based on the jet-hole diameter d and sonic jet mean speed U_j, ranged from 1.25×10^4 to 5.83×10^4 for the range of P_{oj} tested. Table 1 shows the flow details related to micro air jets in Mach 2 flow ($P_\infty = 23$ KPa). The level of underexpansion P_i/P_∞ varied from 3.2 to 14.3, while the momentum flux ratio q varied from 0.77 to 3.43 for the range of P_{oj} tested. Initially, tests with both AJVG1 and AJVG2 were conducted for a ramp angle $\theta = 24$ deg. Later, tests with AJVG2 were also extended for θ of 22 and 20 deg. The no-control case in this paper refers to the test condition with microjet insert (of each configuration) in position but with no airflow or airflow turned off.

The array of microjets was supplied with dry nitrogen gas through eight polyamide tubes of 3 mm diameter, each plugged into a stagnation chamber (to avoid air-jet differences). The pressure P_{oj} inside the stagnation chamber is carefully monitored and used as a parameter to control the AJVG during tests. This chamber in turn was fed by nitrogen gas from a 48 liter bottle stored at 14 MPa. The experimental uncertainty of time-averaged surface-pressure measurements is of the order of $\pm 1\%$. However, in the intermittent region of separation that is associated with high levels of flow unsteadiness (typical rms of 2%), the average pressure uncertainty is likely to be somewhat greater.

B. Signal Conditioning and Data-Acquisition System

Simultaneous wall-pressure measurements along the centerline were made using fast piezoresistive transducers (models XT-140M and XCQ-093). These transducers have a pressure-sensitive area of 0.071 cm and an outer casing diameter of 0.26 and 0.24 cm, respectively. According to the manufacturer's specifications, these transducers have a natural frequency of approximately 250 kHz. The sensitivity of the transducers is typically 3–4 mV/psi. These transducers were calibrated statically. Nine transducers were mounted upstream of the corner with a pitch of 5.5 mm while six of them were mounted on the ramp surface (with a pitch of 5 mm), as shown in Fig. 2. The transducer data were acquired using truly simultaneous data acquisition card NI4495 dc series (with 24 bit resolution) at a sampling frequency of 50 kHz. Each sensor was powered by a dc power supply, and the signal was passed through an amplifier and a signal conditioner. A low-pass filter of 20 kHz was applied during data processing. For each transducer channel, 200 records of 4096 point were acquired, yielding a total of 819,200 data points per channel per tunnel run. For spectral analysis, a 4096 point narrowband fast Fourier transform was performed and later averaged for 200 records, giving a frequency resolution of 12.2 Hz. To access the magnitude of electronic noise in the signals, a simple test was performed. Data were acquired with pressure transducers exposed to a constant pressure (so that ideally no

Table 1 Micro-air-jet flow details in a Mach 2 cross flow; all pressures are in absolute values

P_{oj}, kPa	P_{oj}/P_∞	P_j, kPa	P_j/P_∞	q
139.6	6.07	73.7	3.21	0.77
208.5	9.06	109.6	4.77	1.15
298.2	12.96	157.2	6.85	1.64
367.1	15.96	193.7	8.44	2.03
505.0	21.95	266.1	11.6	2.78
642.9	27.95	328.2	14.3	3.43

fluctuations are recorded) and with same instrument settings as for wind-tunnel tests. The data so acquired were processed in the same way as the fluctuating pressure signals during the test runs. The rms noise-pressure levels were then compared with the rms level measured for the undisturbed boundary layer. The rms noise was found to be approximately $\frac{1}{4}$ of the rms level beneath the Mach 2 undisturbed boundary layer.

The schlieren system used in the study is a Z-type setup where the continuous illumination source is provided by a halogen lamp (250 W) light source (with an effective light-source slit of 1 mm width) and uses two 3.0-m-focal-length spherical mirrors to collimate and refocus the illumination source at the knife-edge location. A vertical-band RGB color filter was used at the knife-edge location and ahead of the camera to capture the flowfield interaction. The color filter was adjusted in a way that the green color represents refractive index gradient near zero. Schlieren images were captured using a Nikon 1X digital camera with a 300 mm zoom lens. The exposure time was set at 125 μs. A mixture of titanium dioxide (TiO_2) powder and vacuum pump oil with a few drops of oleic acid (to improve the dispersion of the pigment in oil) is used for surface oil visualization. The mixture was then sprinkled on the model using a tooth brush.

III. Results and Discussions

A. Flow Visualization

Figures 5 and 6 show the color schlieren images and their corresponding surface oil pictures for the test cases without and with flow control, for both the AJVG1 and AJVG2 configurations, respectively. For the case of no control (Fig. 5a), the flowfield upstream of the interaction is seen to be very clean except for a few weak waves (inclined at 30 deg, which is the Mach angle for Mach 2 flow) visible upstream of the interaction. These are generated by the presence of the insert with no control and do not seem to introduce perturbations in the boundary layer. The interaction region is characterized by a λ shock pattern consisting of separation and reattachment shocks that merge to form an interaction point (I) above the ramp section (marked by a dashed circle). Both types of microjet arrangements are seen to generate local flow perturbations in the form of compression and expansion waves followed by recompression. It is observed that the angle of the shockwave, generated as a result of the micro-air-jet interaction in supersonic cross flow ahead of both micro-AJVG configurations, increases with increase in P_{oj} for each case (and is indicated by the increase in vertical extent of this shock and marked by a dashed ellipse), as shown in Figs. 5b–5d and 6b–6d. Further, the effect of jet penetration into the main flow can also be seen to be more pronounced for the AJVG1 configuration for which a significant increase in the control-generated wave turning angle ζ is seen with increase in P_{oj}, as shown in Figs. 5b–5d. For the AJVG2 configuration, this effect seems to be significantly reduced at all values of P_{oj} tested (Figs. 5d and 6d).

A possible explanation is that a 90-deg-pitched sonic micro air jet is, relatively, able to penetrate more into the main flow (because it presents itself as a larger blunt-body obstruction perpendicular to the supersonic cross flow) than a 45-deg-pitched sonic micro air jet. Figures 7a–7e illustrate the expected general flow features (based on previous studies [35–37]) of an underexpanded jet without and with supersonic cross flow and for both 90- and 45-deg-pitched micro air jets. Further measurements are needed, however, to corroborate this for the present conditions. It may be pointed out that the level of underexpansion for the microjets in the presence of a supersonic cross flow varied from 3.2 to 14.3 for the range of P_{oj} tested, as shown in Table 1. From earlier studies [35,37], it is known that, for levels of underexpansion greater than 6, a Mach disk followed by

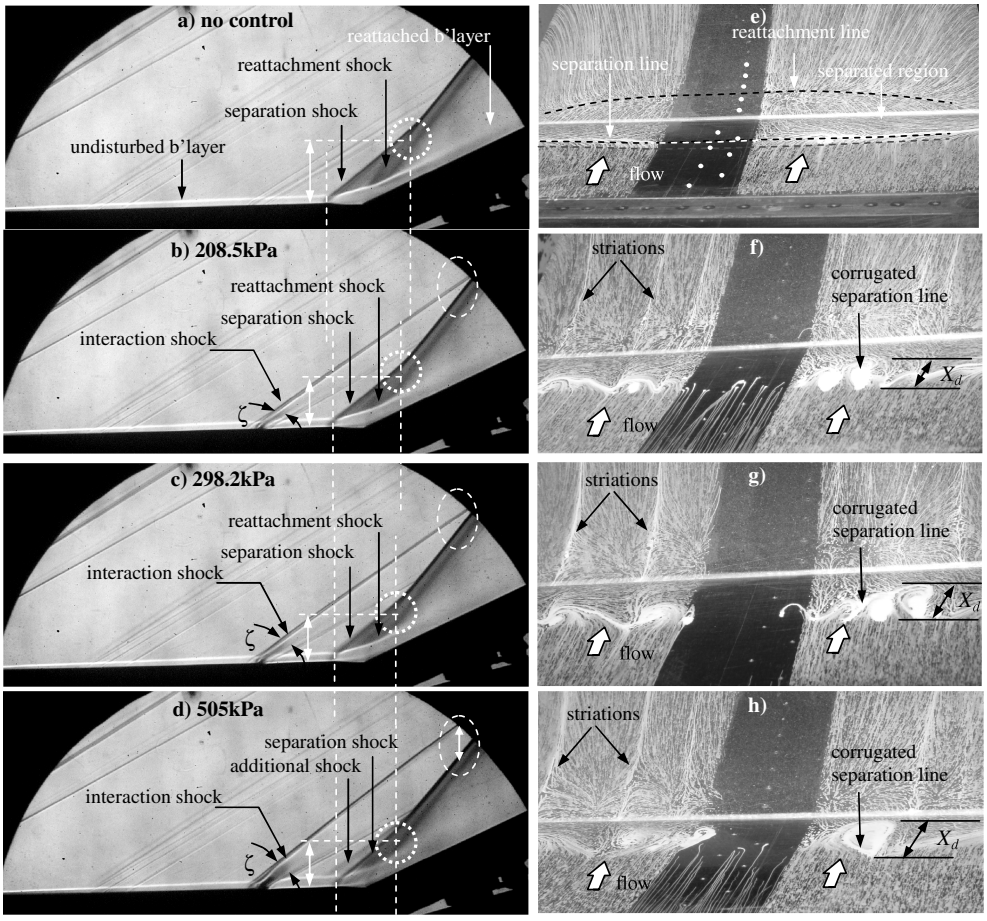

Fig. 5 Schlieren images and the corresponding surface-oil pictures of the flow with AJVG1 for a) and e) no control, b) and f) $P_{oj} = 208.5$ kPa, c) and g) $P_{oj} = 298.2$ kPa, and d) and h) $P_{oj} = 505$ kPa.

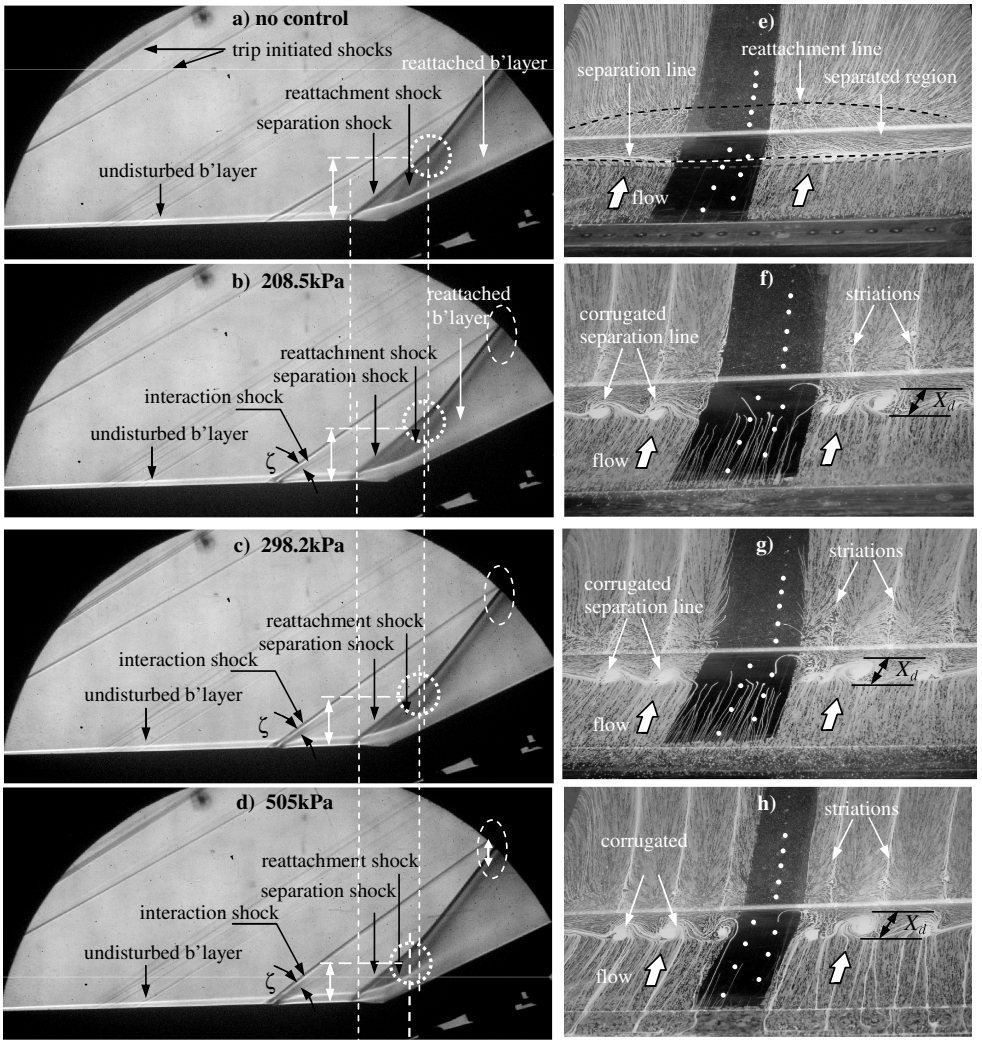

Fig. 6 Schlieren images and the corresponding surface oil pictures of the flow with AJVG2 for a) and e) no control, b) and f) $P_{oj} = 208.5$ kPa, c) and g) $P_{oj} = 298.2$ kPa, and d) and h) $P_{oj} = 505$ kPa.

subsonic flow will always occur. Relative to the no-cross-flow condition (Fig. 7a), a 90-deg-pitched underexpanded jet in a supersonic cross flow produces an inclined barrel shock that terminates in a Mach disk (Fig. 7b). This barrel shock acts as a blunt body obstruction to the incoming flow and results in the formation of a three-dimensional bow shock ahead of the sonic jet. The adverse pressure gradient across the bow shock causes the upstream wall boundary layer to separate, thereby providing a region of interaction upstream of the jet exit. The barrel shock terminates in a Mach disk, and counter-rotating jet-wake vortices are generated as the jet moves downstream [37]. A secondary shock is also formed in the jet wake as a part of the pressure recovery process. The strength of the bow shock varies depending on its location relative to the barrel shock. It is the strongest immediately ahead of the barrel shock (where it is basically a normal shock) and reduces in strength as the bow shock curves downstream in both the lateral and vertical directions, forming a wrapping surface around the barrel shock [35]. On the other hand, for a micro air jet pitched at 45 deg with respect to the wall, the opening at the wall surface (i.e., the jet hole) is an elliptic hole with its minor axis aligned in the direction of the flow and vice versa, as shown in Fig. 4. Thus, in this case, the cross flow actually sees the sonic jet flow development from the major axis plane (Fig. 7c). It is known that the flow development of a sonic underexpanded elliptic jet is different along each plane [36], as shown in Figs. 7c and 7d (i.e., the jet shrinks along its major axis plane while it grows along the minor axis plane as it develops downstream). As a result, in this case, the jet penetration in a supersonic cross flow is much less than that for a 90-deg-pitched jet (Fig. 7e). This effect is also clearly seen from the difference in control-generated shockwave turning angle ζ for each case, as marked in Figs. 5d and 6d.

Figures 8 and 9 show a zoom of the schlieren images taken for AJVG1 and AJVG2 without cross flow and with cross flow, respectively. In the absence of cross flow (Fig. 8), it can be seen that the jet in the AJVG1 configuration (operating at $P_{oj} = 298.2$ kPa) is able to penetrate significantly higher into the quiescent air (Fig. 8a) relative to the jet in the AJVG2 configuration ($P_{oj} = 298.2$ kPa), as expected due to the difference in their pitch angles (Fig. 8b). Even at higher jet operating pressure (i.e., $P_{oj} = 642.9$ kPa), the jet in the AJVG2 configuration penetrates significantly lower than that observed in the AJVG1 configuration for $P_{oj} = 298.2$ kPa (Figs. 8a and 8c). It can also be seen that, in the presence of a supersonic cross flow (Fig. 9), AJVG1 results in a much larger separation region ahead of the injector that is accompanied by a stronger bow shock (higher shock angle), Fig. 9a, relative to AJVG2 (Fig. 9b). Aft of the interaction, a strong secondary shock for AJVG1 in the region of pressure recovery is also indicated (Fig. 9a). The overall comparison of the schlieren images in Fig. 9 indicates that the obstruction component of jet interaction (defined as λ shock region plus overexpansion or low-pressure region [35]) is much larger for AJVG1 relative to AJVG2. Further, the boundary-layer thickness aft of the AJVG1 seems to be relatively higher than that seen for AJVG2. These variations can alter the process of wake development (low-pressure region) and, hence, the generation of counter-rotating vortices in each case. The variation in the surface oil pattern, in the region of separation, in each case (discussed later) is suggestive of changes in wake development due to the variation in AJVG pitch

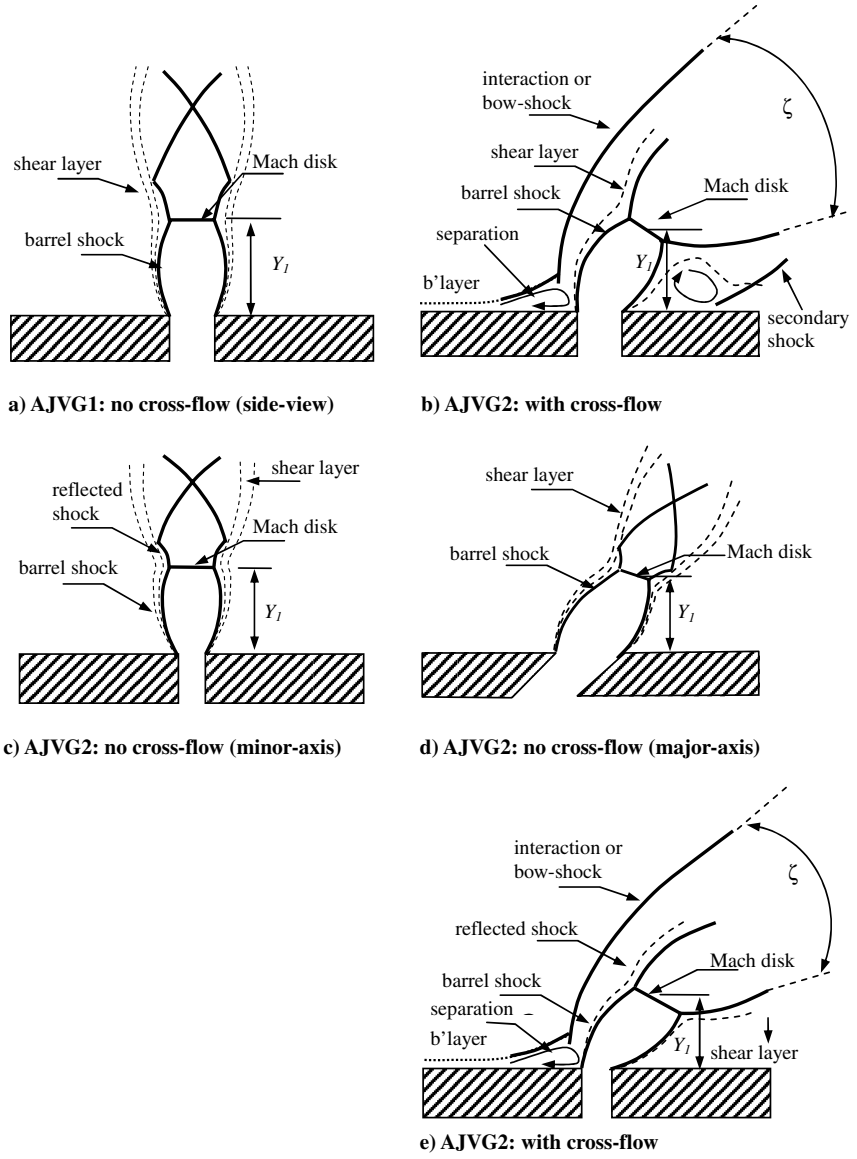

Fig. 7 Schematic of the proposed flow features from AJVGs in the absence and presence of freestream or cross flow based on previous studies [35–37].

angle. The surface oil pattern, immediately downstream of a pair of micro air jets in the AJVG2 configuration, shows the important surface flow features (Fig. 9c). Here, S1 is primary separation, S2 is secondary separation, and S3 is tertiary separation.

It is worthwhile mentioning here that, although schlieren images are instantaneous images of an unsteady flow, the overall modifications in the shock structure with control can still be identified.

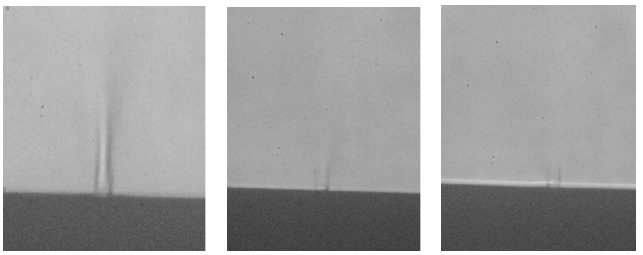

a) b) c)

Fig. 8 Schlieren pictures showing the jet penetration effect with pitch angle (no cross flow) for a) AJVG1, $P_{oj} = 298.2$ kPa; b) AJVG2, $P_{oj} = 298.2$ kPa; and c) AJVG2, $P_{oj} = 642.9$ kPa.

For both micro-AJVG configurations, relative to no control, the separation shock is seen to move downstream while the interaction point (I) moves upstream, thereby reducing the height of the lambda-wave triple point (Figs. 5a, 5b, 6a, and 6b). In addition to this, a significant decrease in the height of the interaction point is also observed with control. Increasing the P_{oj} value beyond 298.2 kPa, however, does not alter these distances any further for AJVG1. However, an additional shock begins to form ahead of the separation shock for $P_{oj} > 298.2$ kPa. At $P_{oj} = 298.2$ kPa (Fig. 5c), this is visible as an initial 'blurring' of the front portion of separation shock, which at $P_{oj} = 505$ kPa can be clearly seen as an additional shock formed ahead of separation shock, as shown in Fig. 6d. On the other hand, for AJVG2, although the separation shock does not move further downstream with increasing P_{oj} (beyond 298.2 kPa, as was also observed for AJVG1), the height of the interaction point (I) as well as its distance from the ramp corner (shown by vertical dashed lines) continues to decrease with further increase in P_{oj} (Figs. 6b–6d).

A comparison of the surface oil pictures of the interaction region reveals significant modifications in the surface flow pattern without and with control (Figs. 5e–5h and 6e–6h). As can be seen from the oil-flow pictures for no control (Figs. 5e and 6e), the flow is not completely two-dimensional. This is because no fences were placed to facilitate schlieren flow visualization with and without control. As

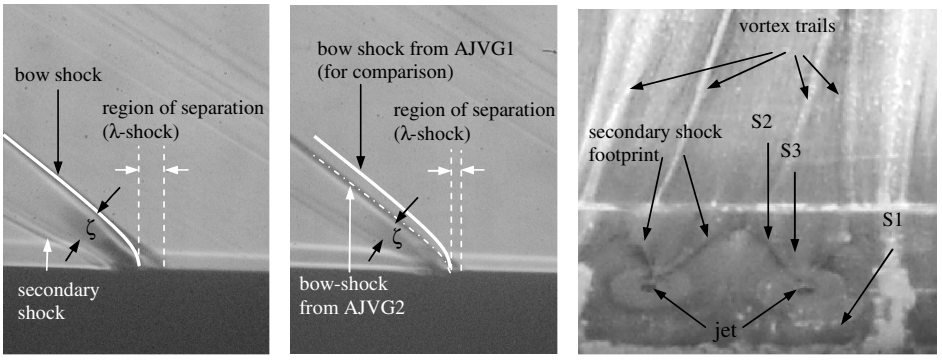

a) b) c)

Fig. 9 Schlieren images showing the jet penetration effect for a) AJVG1, and b) AJVG2; c) oil picture showing important surface flow features for AJVG2 in cross flow; $P_{oj} = 642.9$ kPa.

a result of this, flow spillage occurs from the sides of the flat plate, resulting in an elliptical separation line. A well-defined separation line for the case of no control (Figs. 5a and 6a) is seen to get replaced by a highly corrugated separation line for both AJVG configurations (Figs. 5b and 6b). Upstream of the interaction, trails of streamwise counter-rotating vortex pairs (CVPs) are clearly indicated by the streamwise accumulation of oil pigment (Fig. 6b). Figures 10a and 10b show the upstream view of how the jets in cross flow produce streamwise vortices from each AJVG configuration. These schematics are proposed based on the results from previous studies [19,26,33,37]. Although both AJVG configurations are known to generate streamwise CVP, pitching the jets in the counter-rotating configuration produces streamwise CVP with different strengths on the inward and outward sides [19], as shown in Fig. 10b. Further detailed measurements are needed, however, to corroborate the variation in flow physics from each configuration for the present test conditions. Figure 10c shows a schematic of the flow development leading to the formation of a corrugated surface flow pattern, as developed from surface oil studies. The inset in Fig. 10c shows a surface oil picture with vital surface flow features as obtained after a short test run (of 8 s). As can be seen, the corrugated separation line is formed as a result of the interaction between the streamwise CVP and the reverse flow in the separated region (separation bubble). In the region of the upwash of the vortices (region of low-shear), the reverse flow is able to penetrate into the main flow, whereas in the region of the downwash (region of high-shear) the main flow is able to penetrate into the region of reverse flow. On the other hand, a well-defined reattachment line for the no-control case is also seen to be completely replaced by a striation pattern (beginning from ramp corner itself) with each striation originating exactly in line with the location of each crest of the corrugated separation line. The origin of these striations is, therefore, different from those originating due to generation of Görtler vortices in reattaching boundary layers.

The variation in pitch angle and, hence, in the jet penetration height also seems to have some influence on the flow topology. As discussed previously, the obstruction component of jet interaction is considerably higher for AJVG1 relative to AJVG2. As a result, for AJVG1 the spanwise extent of wake development will be much higher than that for AJVG2 and, hence, will affect the number of corrugations formed in the separation line. A careful examination of the surface flow patterns reveals that, when the AJVG2 configuration is used, the flow pattern seems to develop more corrugations/striations than that observed using the AJVG1 configuration. This variation may also be due to the differences in wake-flow development from each of these configurations, as depicted in Figs. 10a and 10b. Further, the streamwise length of the corrugations (X_d) as well as their lateral extent seems to be affected more by increase in P_{oj} for the AJVG1 configuration than for the AJVG2 configuration.

B. Streamwise Mean Pressure Distribution

Figures 11a–11d show the streamwise distribution of mean pressure (P_w/P_∞) and its corresponding rms value (σ/P_w) for AJVG1 and AJVG2, respectively, as a function of injection pressure P_{oj}. The no-control case here refers to the test condition with microjet insert (of each configuration) in position but with no airflow or with airflow turned off. A careful observation shows slight discrepancies in the wall pressure distributions for the cases with no control for AJVGI and AJVG2 inserts in position (Figs. 11a and 11c). These differences may arise due to discrepancies in placing the new

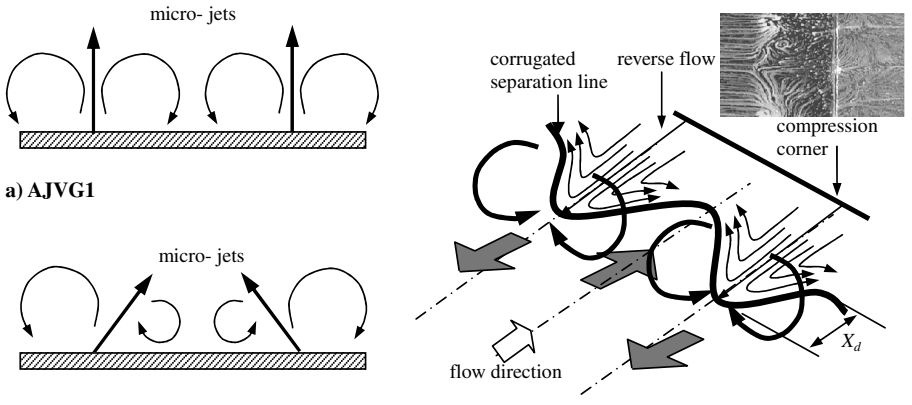

Fig. 10 Schematic showing a–b) the longitudinal vortices expected to be generated by the AJVG1 and AJVG2 configurations [19], respectively, and c) the proposed development of the corrugated surface flow pattern.

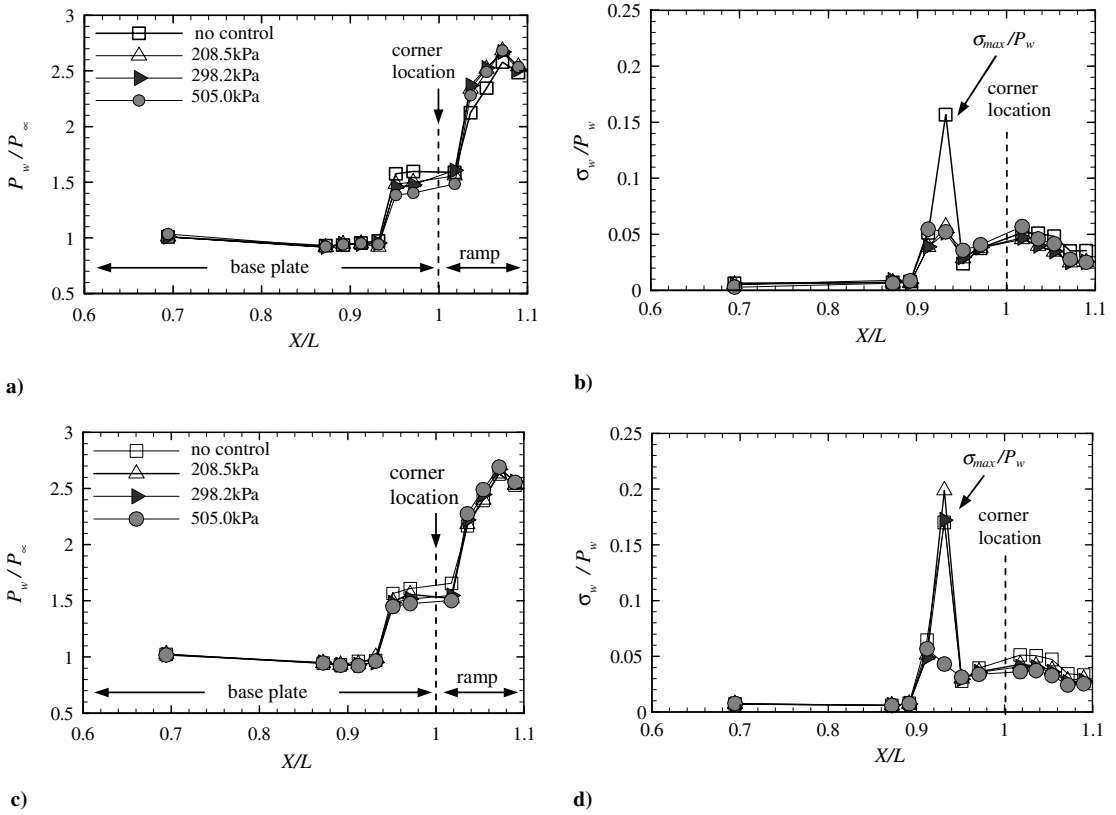

Fig. 11 Streamwise distribution of mean pressure and the corresponding rms value as a function of injection pressure for a–b) AJVG1, and c–d) AJVG2.

insert (with a different microjet configuration) flush with the flat plate. Relative to no control, the rise in wall pressure in the region of separation is observed to decrease for both AJVG configurations (Figs. 10a and 10c) with increase in P_{oj}. However, for the AJVG1 configuration, this decrease seems to be slightly more than that observed for the AJVG2 configuration (showing only a modest gain). The corresponding rms distributions show a significant reduction in the value of peak rms ($\sigma_{\max}/P_w$) in the region of intermittent separation for both configurations (Figs. 11b and 11d). However, in the region of reattachment on the ramp surface, σ/P_w distribution is seen to show slightly higher values with AJVG1 and lower values with AJVG2 relative to no control. These changes in streamwise distribution of rms value in the region of interaction suggest significant changes in the region of interaction and, hence, in the associated flow development process.

Figure 12 shows the plot of peak rms value plotted as a function of injection pressure P_{oj} for both configurations of injectors. Each test was repeated twice, and the repeatability of the rms values was roughly within ± 0.02. Once again, it can be seen that, due to the larger obstruction component of AJVG1, a significant reduction in the $\sigma_{\max}/P_w$ value is obtained compared to no control as soon as control is applied, up to 67% reduction for $P_{oj} \geq 208.5$ kPa (Fig. 12a), due to reasons discussed previously. Thereafter, this value is seen to remain almost constant. However, for AJVG2, the $\sigma_{\max}/P_w$ value initially shows an increase (for P_{oj} up to 208.5 kPa) after which it begins to decrease with increase in P_{oj} (Fig. 12b). At $P_{oj} = 298.2$ kPa, the $\sigma_{\max}/P_w$ value is similar to that measured for no control. As P_{oj} is further increased, a significant reduction in $\sigma_{\max}/P_w$ value (up to 67% for $P_{oj} = 505$ kPa), similar to that for AJVG1, is observed. Tests with AJVG2 were also extended for θ of 22 and 20 deg to further investigate the effectiveness of this flow-control technique. A similar trend of $\sigma_{\max}/P_w$ variation with P_{oj} is observed for $\theta = 22$ deg as observed for ramp angle of 24 deg (Fig. 12b). However, for $\theta = 20$ deg, the AJVG2 configuration does not seem to be very effective as the peak rms values with control remains almost similar to that observed for no control.

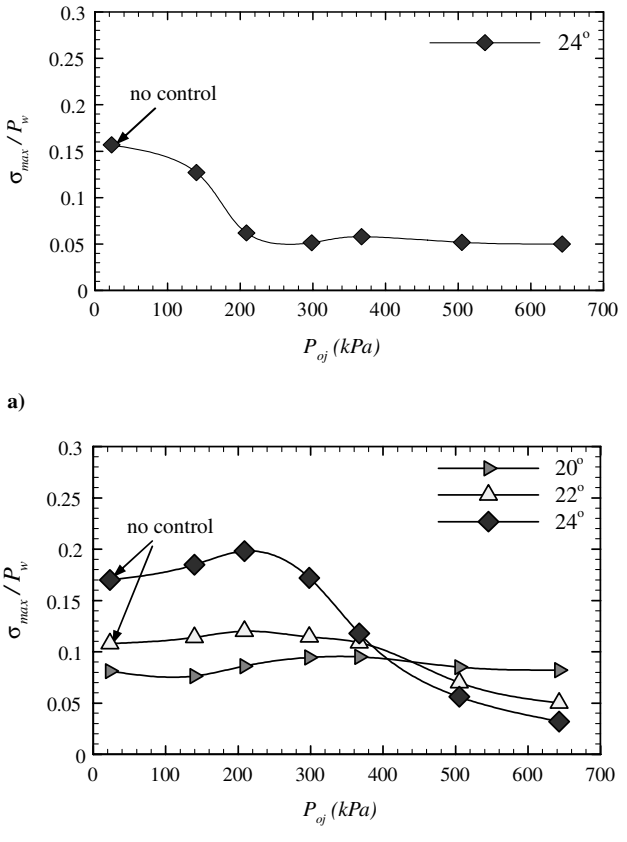

Fig. 12 Variation of peak rms value in the intermittent region of separation as a function of injection pressure for a) AJVG1, 24 deg, and b) AJVG2.

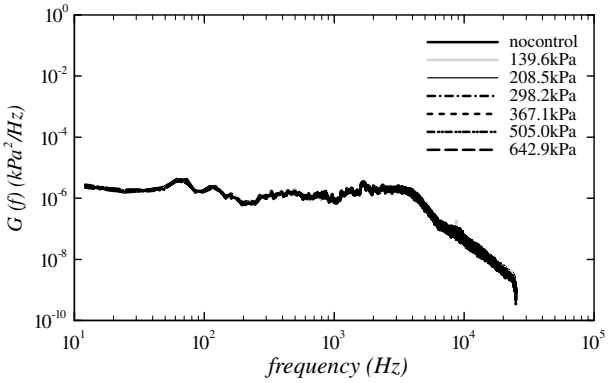

Fig. 13 Spectra content of the undisturbed boundary layer ($X/L = 0.694$) ahead of control as a function of injection pressure $\theta = 24$ deg.

Because flow unsteadiness in SWBLI is known to decrease with decrease in shock strength [3,5,6,8,9,26], a reduction in $\sigma_{\max}/P_w$ value in the region of intermittent region of interaction is an indication of a weaker separation shock. From this point of view, AJVG1 is a better control configuration than AJVG2 as a significant reduction in $\sigma_{\max}/P_w$ is obtained as soon as control is applied. Similar results with AJVG2 are achieved but for much higher values of injection pressure ($P_{oj} \geq 505$ kPa). As discussed, this could be due to the fact that the AJVG1 configuration generates a much higher obstruction component than AJVG2 as seen in Figs. 9a and 9b. As a result, AJVG1 is able to influence the flow laterally more than that done by AJVG2. This causes AJVG1 to stabilize the flow much earlier, whereas this happens for AJVG2 at a much higher P_{oj}.

C. Spectral Analysis

Figure 13 shows the spectra of wall pressure in the undisturbed boundary layer while Figs. 14 and 15 show the streamwise evolution of spectra of wall pressure fluctuations in the region of separation and reattachment locations as a function of air-jet injection pressure P_{oj} for both the AJVG1 and AJVG2 configurations, respectively. It may be pointed out that, for the present test conditions, the characteristic frequency (U_e/δ) of energetic scales in the incoming boundary layer is approximately 130 kHz. The Strouhal number ($St = f_s L_s/U_e$) for compression ramp flows generally lies between 0.02 and 0.05 [4,6] (where L_s is the length of separation). Therefore, for the present test case, the characteristic frequency of shock motion lies between 500 and 1300 Hz, or 0.004 $0.004U_e/\delta$ to $0.01U_e/\delta$. It can be seen in general that, relative to the spectra of the undisturbed boundary layer (Fig. 13), a dramatic increase in energy levels (by three orders of magnitude) is observed in the intermittent region of separation (which is located at the point of maximum rms level) where the wall pressure signal is dominated by relatively low-frequency, high-amplitude pressure fluctuations due to the back-and-forth unsteady motion of the separation shock (Figs. 14a and 15a). Thereafter, a steep drop in the slope of the spectra occurs beyond 1 kHz for AJVG1 and 2 kHz for AJVG2. This shows that the pressure fluctuations in the region of separation are dominated more by shockwave oscillations than by the incoming turbulence. No coherent shock-motion frequencies are evident. Further downstream and under the separation bubble, the amplitude of low-frequency pressure fluctuations are seen to drop with a subsequent increase in the amplitude of high-frequency content of the spectra (Figs. 14b and 15b). The latter could be due to the nature of turbulent structures being convected in the separated shear layer. However, the dominance of low-frequency high-amplitude pressure fluctuations is preserved even in the region of separation bubble and up to the reattachment location (Figs. 14c and 15c). In the region of reattachment, the spectra show a slight drop in the energy levels of the low-frequency pressure fluctuations. At the same time, the high-frequency (up to 10 kHz) high-amplitude pressure fluctuations of the turbulent shear-layer are seen to contribute toward a large fraction of the pressure signal at this location. Thereafter, a sharp drop in the energy levels is seen beyond 10 kHz.

Applying control helps to reduce the amplitude of pressure fluctuations in the separation location for both AJVG configurations (Figs. 14a and 15a) and is seen to reduce significantly with increase in P_{oj}. This trend is consistent with the results of shock unsteadiness

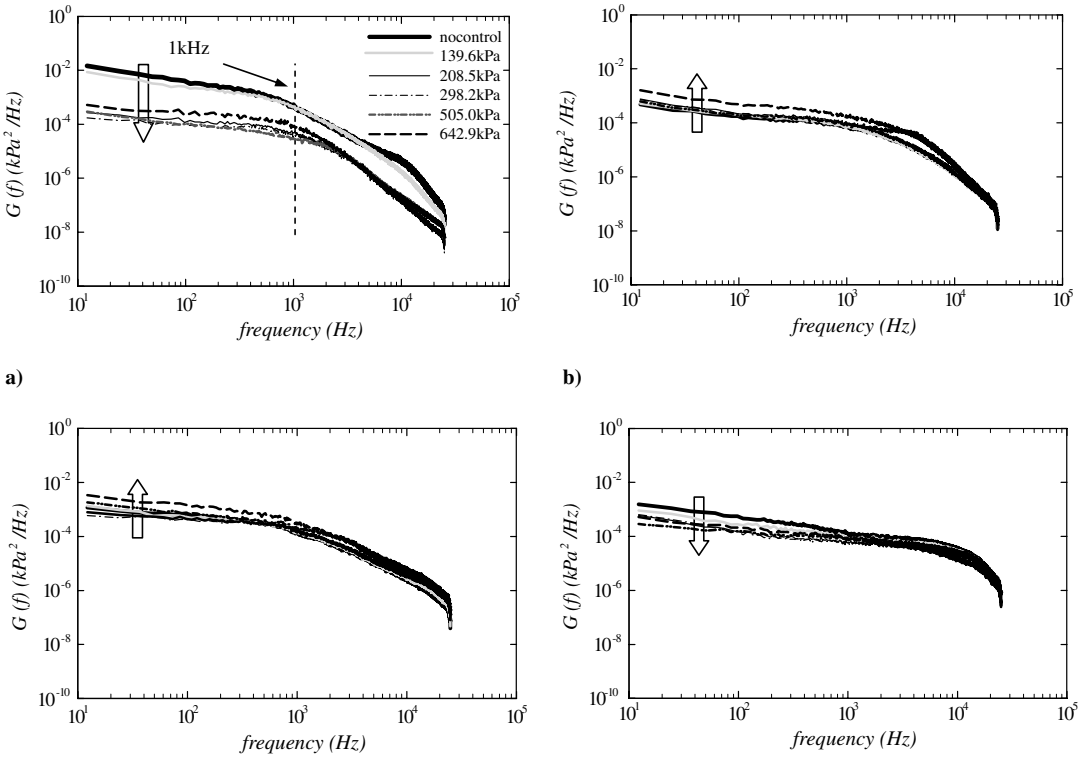

Fig. 14 Comparison of spectra: a) the intermittent region of separation ($X/L = 0.931$), b) inside the separation bubble ($X/L = 0.97$), c) vicinity of reattachment ($X/L = 1.03$), and d) downstream of reattachment ($X/L = 1.07$); $\theta = 24$ deg, AJVG1.

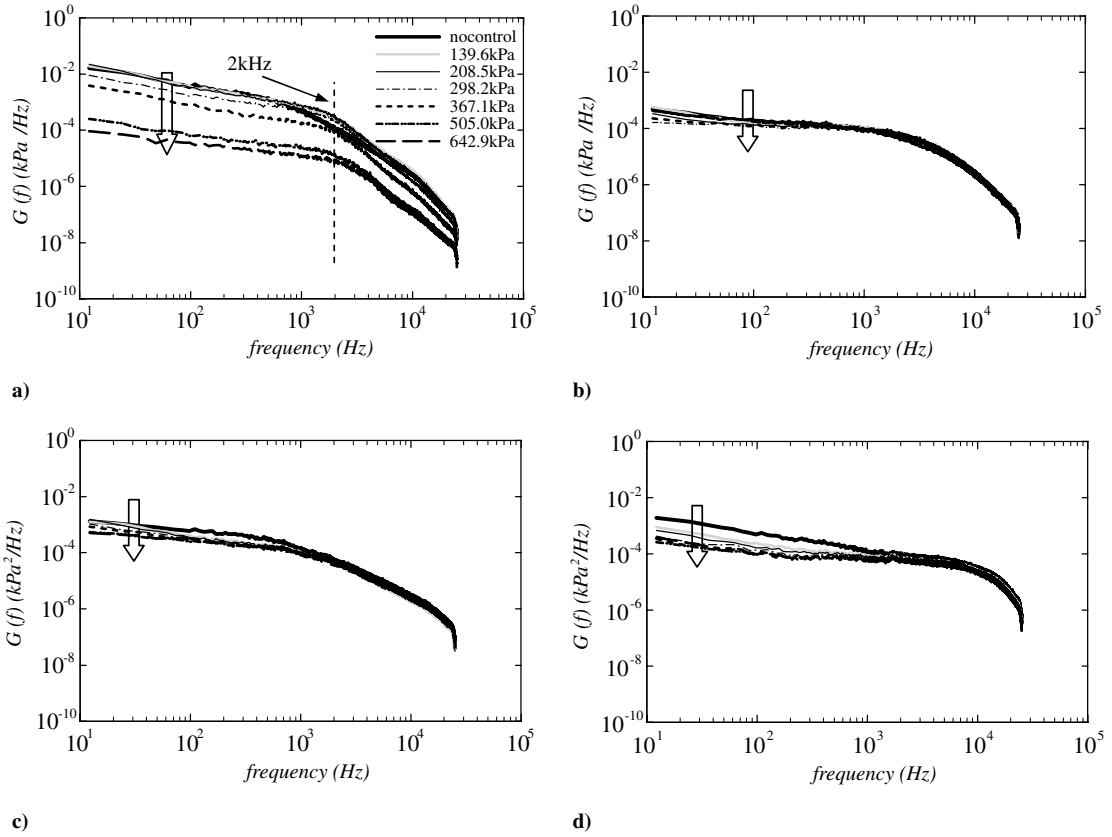

Fig. 15 Comparison of spectra: a) the intermittent region of separation ($X/L = 0.931$), b) inside the separation bubble ($X/L = 0.97$), c) vicinity of reattachment ($X/L = 1.03$), and d) downstream of reattachment ($X/L = 1.07$); $\theta = 24$ deg, AJVG2.

shown in Figs. 11b and 11d. A similar trend is also observed for ramp angles of 20 and 22 deg with the AJVG2 configuration (Figs. 16a and 16b). The slope of the spectra in the range of unsteadiness (500–1300 Hz) is observed to be approximately −1 and is seen to remain the same, with and without control. However, beyond 2 kHz, the slope of the spectra shifts from −2 for no-control case to −3 with control. This suggests that applying flow control not only helps to reduce the amplitude of low-frequency shock motions but also modifies the nature of turbulent structures being convected downstream. However, for the AJVG1 configuration, in the region of separated flow (separation bubble) and reattachment, the amplitude of pressure fluctuations is seen to slightly increase with increasing P_{oj}. On the other hand, using the AJVG2 configuration is seen to consistently reduce the pressure fluctuations in these regions as well. Finally, downstream of reattachment, both AJVG configurations show significant reduction in pressure fluctuations with increasing P_{oj} in the entire frequency range. These observations suggest that both AJVG configurations are successful in reducing the separation shock unsteadiness and amplitude of pressure fluctuations.

The results indicate that both micro-AJVG configurations act as effective flow control devices in controlling a Mach 2 shockwave/boundary-layer interaction on a 24 deg compression corner. Both micro-AJVG configurations are observed to reduce the separation shock strength with the primary objective of reducing the shock unsteadiness. However, pitching the air jets to 45 deg (in a counter-rotating configuration) causes the jets to penetrate significantly lesser into the main flow relative to the AJVG1 configuration. This prevents a stronger control-generated bow shock to form ahead of the air jets and, hence, helps to reduce the obstruction component of the control significantly. Further, AJVG2 also helps to reduce the height of the lambda-wave triple point with increase in P_{oj}. The spectral content of the pressure fluctuations indicate that, compared to the AJVG2 configuration, AJVG1 is more successful in reducing the amplitude of fluctuations as soon as control is applied, which is also consistent

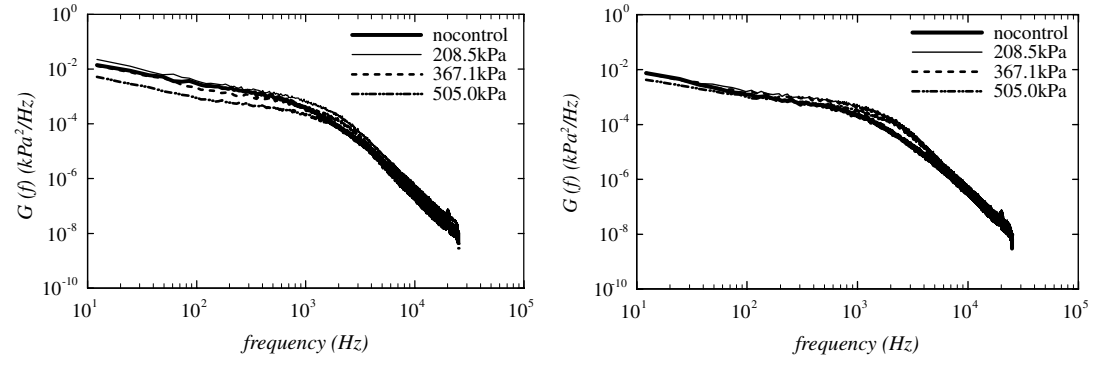

Fig. 16 Comparison in the variation in spectral content of the pressure signal as a function of injection pressure (AJVG2) in the intermittent region of separation ($X/L = 0.931$) for a) $\theta = 22$ deg and, b) $\theta = 20$ deg.

with the results of shock unsteadiness. These results suggest that the use of microjets in a supersonic cross flow for the purpose of flow control is an effective flow-control technique and helps in mitigating the adverse effects of SWBLI on a compression corner.

IV. Conclusions

An experimental test campaign was conducted to study the effectiveness of micro-air-jet vortex-generating (AJVG) devices in controlling the amplitude of shock unsteadiness associated with a 24 deg compression ramp-induced interaction in a Mach 2 flow. Two control configurations in the form of an array of 1) 16 90-deg-pitched steady micro air jets (AJVG1), and 2) eight pairs of 45-deg-pitched (pairs arranged in counter-rotating configuration) steady micro air jets (AJVG2) were studied. Each of these control devices were introduced upstream of the interaction region at 12.5δ from the corner. The interaction is studied using color schlieren, fast piezoresistive Kulite pressure sensors, and surface-oil flow.

For both AJVG configurations, relative to no control, the separation shock is seen to move downstream while the interaction point (I) moves upstream. This reduces the height of the lambda-wave triple point. Although the separation shock does not move further downstream with increasing P_{oj} for both AJVG configurations, unlike AJVG1, with AJVG2 the height of the interaction point (I), as well as its distance from the ramp corner, continues to further decrease with increase in P_{oj}. Also, due to the higher pitch angle, air jets in the AJVG1 configuration penetrate significantly more into the supersonic cross flow relative to the air jets in the AJVG2 configuration, causing a stronger bow shock to form ahead of the injectors. This causes the obstruction component of jet interaction to be much larger for AJVG1 relative to AJVG2. As a result, pitching the micro air jets at 45 deg as in the AJVG2 configuration prevents a stronger control-generated shock to form ahead of the injectors and also helps to significantly reduce the height of lambda-wave triple point.

A well-defined separation line for no control is seen to get replaced by a highly corrugated separation line with control. The reattachment line, however, shows no sign of corrugations. But on the ramp surface and in the vicinity of the reattachment region, a well-defined reattachment line (for no control) gets replaced by a clearly formed striation pattern with control. Comparison with the no-control case shows that the origin of these striations is not due to the formation of Görtler vortices (as is usually the case with reattaching boundary layer) but due to the flow modifications induced downstream of the corrugated separation line. Also, due to the larger obstruction component, the spanwise extent of wake development for AJVG1 is much higher than that for AJVG2 and, hence, affects the number of corrugations formed on the separation line. Increasing P_{oj} also increases the depth X_d as well as the lateral extent of the corrugations with AJVG1, while these are observed to remain unaffected when AJVG2 is used.

The rise in wall pressure P_w in the region of separation is observed to decrease for both AJVG configurations with increase in P_{oj}. But because of the larger obstruction component for AJVG1, a significant reduction in the $\sigma_{\max}/P_w$ value is obtained compared to no control as soon as control is applied (up to 67% reduction for $P_{oj} \geq 208.5$ kPa. However, for AJVG2, the $\sigma_{\max}/P_w$ value initially (for P_{oj} up to 208.5 kPa) shows an increase after which it begins to decrease, and for $P_{oj} \geq 505$ kPa the $\sigma_{\max}/P_w$ value shows significant reduction in $\sigma_{\max}/P_w$ value (up to 67%), similar to that seen for AJVG1. The spectral content of the pressure fluctuations also indicates that, relative to the AJVG2 configuration, AJVG1 is successful in reducing the amplitude of fluctuations in the range of unsteadiness by an order of magnitude for $P_{oj} \geq 208.5$ kPa. Relative to AJVG2, the overall results with AJVG1 seem to be favorable from the viewpoint of an effective flow control configuration.

Acknowledgments

The authors wish to thank the Aeronautical Research and Development Board of India for supporting this project. The technical support of Ravi Dodamani during the model design and fabrication as well as Perinaygam, Janardhan, and Muthuswamy, staff of the 0.3 m wind tunnel facility at National Aerospace Laboratories (NAL) during the test campaign, is gratefully acknowledged. Special thanks to Gangadhar, Shanmogan, and Charan Singh of the NAL Belur Model Shop for model fabrication.

References

[1] Kistler, A. L., "Fluctuating Wall Pressure Under Separated Supersonic Flow," *Journal of the Acoustical Society of America*, Vol. 36, No. 3, March 1964, pp. 543–550. doi:10.1121/1.1918998

[2] Hadjadj, A., and Dussauge, J. P., "Shock Wave Boundary Layer Interaction," *Shock Waves*, Vol 19, 2009, pp. 449–452. doi:10.1007/s00193-009-0238-2

[3] Dolling, D. S., and Murphy, M. T., "Unsteadiness of the Separation Shock Wave Structure in a Supersonic Compression Ramp Flowfield," *AIAA Journal*, Vol. 21, No. 12, 1983, pp. 1628–1634. doi:10.2514/3.60163

[4] Dolling D. S., "Fifty Years of Shock-Wave/Boundary-Layer Interaction Research: What Next?," *AIAA Journal*, Vol. 39, No. 8, 2001, pp. 1517–1531. doi:10.2514/2.1476

[5] Dolling, D. S., and Or, C. T., "Unsteadiness of the Shock Wave Structure in Attached and Separated Compression Ramp Flows," *Experiments in Fluids*, Vol. 3, 1985, pp. 24–32. doi:10.1007/BF00285267

[6] Muck, K. C., Andreopoulos, J., and Dussuage, J. P., "Unsteady Nature of Shock-Wave/Boundary-Layer Interactions," *AIAA Journal*, Vol. 26, No. 2, 1988, pp. 179–187. doi:10.2514/3.9870

[7] Verma, S. B., "Experimental Study of Flow Unsteadiness in a Mach 9 Compression Ramp Interaction Using a Laser Schlieren System," *Measurement Science and Technology Journal*, No. 7, 2003, pp. 989–997. doi:10.1088/0957-0233/14/7/312

[8] Dolling, D. S., and Bogdonoff, S. M., "An Experimental Investigation of the Unsteady Behavior of Blunt Fin-Induced Shock Wave Turbulent Boundary Layer Interaction," *14th AIAA Fluid and Plasma Dynamics Conference*, Palo Alto, CA, AIAA Paper 1981-1287, June 1981.

[9] Dolling, D. S., and Brusniak, L., "Separation Shock Motion in Fin, Cylinder, and Compression Ramp-Induced Turbulent Interactions," *AIAA Journal*, Vol. 27, No. 6, 1989, pp. 734–742. doi:10.2514/3.10173

[10] Beresh, P. L., Clemens, N. T., and Dolling, D. S., "Relationship Between Upstream Turbulent Boundary-Layer Velocity Fluctuations and Separated Shock Unsteadiness," *AIAA Journal*, Vol. 40, No. 12, 2002, pp. 2412–2422. doi:10.2514/2.1609

[11] Ganapathisubramani, B., Clemens, N. T., and Dolling, D. S., "Effects of Upstream on the Unsteadiness of Shock Induced Separation," *Journal of Fluid Mechanics*, Vol. 585, Aug. 2007, pp. 369–394. doi:10.1017/S0022112007006799

[12] Maull, D. J., "Hypersonic Flow over Axially Symmetric Spiked Bodies," *Journal of Fluid Mechanics*, Vol. 8, No. 4, 1960, pp. 584–592. doi:10.1017/S0022112060000815

[13] Charwat, A. F., Dewey, C. F., Roos, J. N., and Hitz, J. A., "Investigation of Separated Flows, Part 2; Flow in Cavity and Heat Transfer," *Journal of the Aerospace Sciences*, Vol. 28, No. 7, 1961, pp. 513–527. doi:10.2514/8.9099

[14] Blinde, P. L., Humble, R. A., Oudheusden, B. W., and Scarano, F., "Effects of Micro-Ramps on a Shock Wave/Turbulent Boundary Layer Interaction," *Shock Waves*, Vol. 19, 2009, pp. 507–520. doi:10.1007/s00193-009-0231-9

[15] McCormick, D. C., "Shock/Boundary-Layer Interaction Control with Vortex Generators and Passive Cavity," *AIAA Journal*, Vol. 31, No. 1, 1993, pp. 91–96. doi:10.2514/3.11323

[16] Bur, R., Coponet, D., and Carpels, Y., "Separation Control by Vortex Generators Devices in a Transonic Channel Flow," *Shock Waves*, 2009, pp. 521–530. doi:10.1007/s00193-009-0234-6

[17] Babinsky, H., Makinson, N. J., and Morgan, N. J., "Micro-Vortex Generator Flow Control for Supersonic Engine Inlets," *45th AIAA Aerospace Sciences Meeting and Exhibit*, Reno, NV, AIAA Paper 2007-0521, Jan. 2007.

[18] Szwabe, R., "Shock Wave Induced Separation Control by Streamwise Vortices," *Journal of Thermal Science*, Vol. 14, No. 3, 2005,

pp. 249–253.
doi:10.1007/s11630-005-0009-z
[19] Souverein, L. J., and Debiève, J.-F., "Effect of Air Jet Vortex Generators on a Shock Wave Boundary Layer Interaction," *Experiments in Fluids*, Vol. 49, 2010, pp. 1053–1064.
doi:10.1007/s00348-010-0854-8
[20] Lin, J. C., "Review of Research on Low-Profile Vortex Generators to Control Boundary-Layer Separation", *Progress in Aerospace Sciences*, Vol. 38, Nos. 4–5, 2002, pp. 389–420.
doi:10.1016/S0376-0421(02)00010-6
[21] Khan, Z. U., and Johnston, J. P., "On Vortex Generating Jets," *International Journal of Heat and Fluid Flow*, Vol. 21, No. 5, 2000, pp. 506–511.
doi:10.1016/S0142-727X(00)00038-2
[22] Kamotani, Y., and Greber, I., "Experiments on a Turbulent Jet in Cross-Flow," *AIAA Journal*, Vol. 10, No. 11, 1972, pp. 1425–1429.
doi:10.2514/3.50386
[23] Zhuang, N., Alvi, F. S., Alkislar, B., and Shih, C., "Supersonic Cavity Flows and Their Control," *AIAA Journal*, Vol. 44, No. 9, 2006, pp. 2118–2128.
doi:10.2514/1.14879
[24] Kumar, V., and Alvi, F. S., "Toward Understanding and Optimizing Separation Control Using Micro-Jets," *AIAA Journal*, Vol. 47, No. 11, 2009, pp. 2544–2557.
doi:10.2514/1.38868
[25] Ali, M. Y., Alvi, F. S., Manisankar, C., Verma, S. B., and Venkatkrishnan, L., "Studies on the Control of Shock Wave-Boundary layer Interaction Using Steady Microactuators," *41st AIAA Fluid Dynamics Conf. and Exhibit*, Honolulu, AIAA Paper 2011-3425, June 2011.
[26] Godard, G., and Stanislas, M., "Control of a Decelerating Boundary Layer. Part 3: Optimization of Round Jets Vortex Generators," *Aerospace Science and Technology*, Vol. 10, No. 6, 2006, pp. 455–464.
doi:10.1016/j.ast.2005.11.005
[27] Johari, H., and McManus, K., "Visualization of Pulsed Vortex Generator Jets for Active Control of Boundary Layer Separation," *28th AIAA Fluid Dynamic Conference*, Snowmass Village, CO, AIAA Paper 1997-2021, Jan. 1997.
[28] McManus, K., and Magill, J., "Separation Control in Incompressible and Compressible Flows Using Pulsed Jets," *27th AIAA Fluid Dynamics Conference*, New Orleans, LA, AIAA Paper 1996-1948, June 1996.
[29] Delery, J. M., "A Physical Introduction to Control Techniques Applied to Turbulent Separated Flows," *Fluids 2000 Conference and Exhibit*, Denver, CO, AIAA Paper 2000-2606, June 2000.
[30] Manisankar, C., Verma, S. B., and Raju, C., "Shock-Wave Boundary-Layer Interaction Control on a Compression Corner Using Mechanical Vortex Generators," *28th International Shock Wave Symposium*, Manchester, UK, 17–22 July 2011, Paper 2446.
[31] Van Driest, E. R., "Turbulent Boundary Layer in Compressible Flows," *Journal of the Aeronautical Sciences*, Vol. 18, No. 3, 1951, pp. 145–160.
[32] Verma, S. B., and Gupta, V., "*Supersonic Separation with Obstructions*," *AIAA Journal*, Vol. 34, No. 4, 1996, pp. 849–850.
doi: 10.2514/3.13151
[33] O'Donnell R. M., "Experimental Investigation at a Mach Number of 2.41 of Average Skin-Friction Coefficients and Velocity Profiles for Laminar and Turbulent Boundary Layers and an Assessment of Probe Effects," NACA TN 3122, Jan. 1954.
[34] Lin, C. C., *Turbulent Flows and Heat Transfer*, Princeton Univ. Press, Princeton, NJ, 1959.
[35] Viti, V., Neel, R., and Schetz, J. A., "Detailed Flow Physics of the Supersonic Jet Interaction Flow Field," *Physics of Fluids*, Vol. 21, No. 4, 2009, pp. 046101-16.
doi:10.1063/1.3112736
[36] Verma, S. B., and Rathakrishnan, E., "Flow and Acoustic Properties of Underexpanded Elliptic-Slot Jets," *Journal of Propulsion and Power*, Vol. 17, No. 1, Jan.–Feb. 2001, pp. 49–57.
doi:10.2514/2.5706
[37] Dickmann, D. A., and Lu, F. K., "Jet in Supersonic Crossflow on a Flat Plate," *25th AIAA Aerodynamic Measurement Technology and Ground Testing Conference*, San Francisco, AIAA Paper 2006-3451, June 2006.

G. Elliott
Associate Editor